Resizing Metal-Coated Nanopores Using a Scanning Electron Microscope

*Guillaume A. T. Chansin, Jongin Hong, Jonathan Dusting, Andrew J. deMello, Tim Albrecht, and Joshua B. Edel**

Electron beam-induced shrinkage provides a convenient way of resizing solid-state nanopores in Si_3N_4 membranes. Here, a scanning electron microscope (SEM) has been used to resize a range of different focussed ion beam-milled nanopores in Al-coated Si_3N_4 membranes. Energy-dispersive X-ray spectra and SEM images acquired during resizing highlight that a time-variant carbon deposition process is the dominant mechanism of pore shrinkage, although granular structures on the membrane surface in the vicinity of the pores suggest that competing processes may occur. Shrinkage is observed on the Al side of the pore as well as on the Si_3N_4 side, while the shrinkage rate is observed to be dependent on a variety of factors.

1. Introduction

Solid-state nanopores have been shown to be powerful tools for sensing individual macromolecules in solution.[1] For example, DNA, RNA, and proteins can be driven through nanopores by applying a voltage across the membrane. By doing so, and recording the ionic current as a function of time, in principle every molecule passing through the pore can be detected and quantified.[2] Solid-state nanopores fabricated in silicon nitride (Si_3N_4) and silicon dioxide (SiO_2) substrates were initially developed to mimic the biological pores embedded in lipid bilayers.[2] Although both solid-state and biological pores have their own merits, a major advantage of the solid-state platform is the ease and flexibility of integrating optical or electrical elements on the same device, for example, the addition of metal electrodes near the pore.[3] Additionally, a solid-state membrane can be coated with a metallic film and used for optical detection of analyte molecules translocating through the contained pores.[4,5] Here, the metal film is key in preventing the propagation of excitation light through the membrane. This idea has been previously demonstrated by Chansin et al.[4] where aluminium coated Si_3N_4 membranes were used for fluorescence detection of λ-DNA molecules passing through nanopores approximately 250 nm in diameter. Aluminium was determined to be an excellent coating material in optically thick metal/dielectric membranes on the basis of reflectivity and transmittance characteristics for an excitation wavelength of 488 nm.[5] Importantly, demonstration of such a technique opens the way for the simultaneous operation of multiple nanopores in large arrays. This would represent a significant advantage over conventional ionic current detection where only the signal of one pore can be measured at any given time.

Solid-state nanopores can be fabricated using a number of different methods; however, transmission electron microscopy (TEM) and focussed ion-beam (FIB) milling have proved to be the most popular. TEM enables the drilling of thin membranes made of SiO_2[6] or Si_3N_4[7–10] with high precision. FIB milling is simpler and offers greater flexibility, as pores can be drilled in thicker membranes and other materials such as metals.[11,12] Using a conventional FIB, the minimum pore size is limited to approximately 30 nm for Si_3N_4 membranes.[2] However, it is advantageous to be able to fine-tune the size of the pore below that limit since precise control over pore diameter has been shown to be extremely important in sensor

Dr. G. A. T. Chansin, Dr. J. Dusting, Dr. T. Albrecht, Dr. J. B. Edel
Department of Chemistry
Imperial College London
London, SW7 2AZ, UK
E-mail: joshua.edel@imperial.ac.uk
Dr. J. Hong
Department of Chemistry
College of Natural Science
Chung-Ang University, Seoul, South Korea
Prof. A. J. deMello
Department of Chemistry and Applied Biosciences
Wolfgang-Pauli-Strasse 10, ETH Zurich, CH-8093 Zürich, Switzerland

DOI: 10.1002/smll.201101015

NANO MICRO small

applications, especially in the context of optical readout of DNA sequences.[13] Li et al. implemented an ion detection-based feedback system to improve control over the FIB milling process. Using this system on a bowl-shaped cavity in an Si_3N_4 membrane, they found that the ion beam could also induce shrinkage of the pore from 60 to 1.8 nm.[14]

A shrinkage process also needs to be applied to the FIB-milled pores in metal-coated membranes. One strategy is to reduce the aperture size in a metallic membrane via electrodeposition.[11,12] However, when using fluorescence detection techniques it is not always desirable to confine the probe inside a narrow metallic structure, as fluorescence can be quenched by nonradiative energy transfer to the metal.[15] Another size-reduction strategy involves the selective deposition of additional material inside the pore using energy from a charged beam, as in electron beam-induced deposition (EBID) or ion beam-induced deposition (IBID). Both EBID and IBID typically require a gas-injection system to deliver precursor gases that diffuse and adsorb on the specimen.[16] For example, EBID has been used for the gradual shrinking of nanopores by depositing several layers of SiO_2 successively.[17] A simpler variant of EBID is the deposition of hydrocarbons without a gas-injection system, whereby hydrocarbons present in background oil vapors from the vacuum system serve as a 'contamination resist' for the deposition.[18] Carbon deposition is often responsible for the rectangular 'footprint' left on a specimen after scanning electron microscopy (SEM) imaging. The process is similar to EBID in the sense that hydrocarbons adsorbed on the specimen surface are polymerised by the secondary electrons. Shrinking of nanopores in Si_3N_4 membranes with carbon has already been performed with both TEM[19] and SEM,[20] and the technique can be applied to silicon structures as well.[21] However, it is possible that the actual shrinkage mechanism may be complex, as a number of different processes such as radiolysis[22] or combinations of Joule heating and electron beam-induced migration[23] have been proposed to explain pore shrinkage by SEM.

In the current study, an SEM has been used to shrink pores in aluminium-coated Si_3N_4 membranes. As the pore size of the metal layer affects the electric field used for both the translocation of molecules and fluorescence detection, it is important to determine the level of control achievable using this method. Due to the nature of the EBID process, the ability to shrink dual-layer pores is not guaranteed, as the two materials are likely to have different secondary electron yields, while electron-stimulated desorption may significantly restrict deposition on the Al layer.[24] Furthermore, there is also a need to locally protect the metal around the pore interface from the bulk solution and the translocating molecules. Elemental analysis by energy dispersive X-ray (EDX) spectroscopy is used to confirm that carbon deposition is the main shrinkage mechanism, while SEM imaging has been used to illustrate the variability of the deposition rate.

2. Results and Discussion

Before attempting to shrink pores on metal-coated membranes, the shrinking of pores on a bare 60 nm-thick Si_3N_4 membrane was investigated. A pore of 143 ± 8 nm was milled with FIB and then scanned with SEM at 20 kV. The magnification was 300 000×, corresponding to a scanning area of 894 nm × 671 nm. Scanning was paused every 2 min in order to acquire EDX spectra and measure the pore diameter.

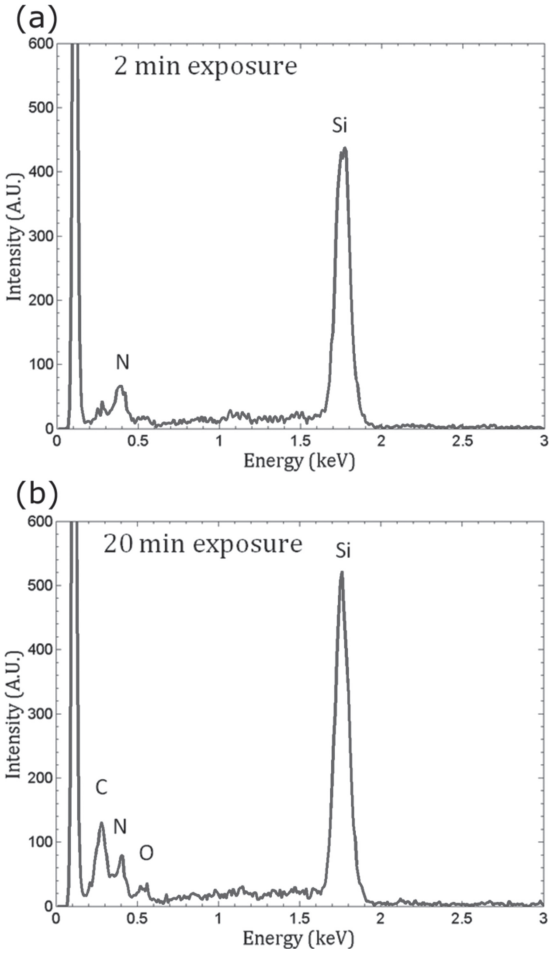

Figure 1. EDX spectra acquired after a) 2 min and b) 20 min of SEM scanning on a Si_3N_4 pore. The acquisition time for each spectrum was 2 min.

Figure 1 shows EDX spectra after 2 and 20 min of electron exposure, and highlights the role of carbon deposition. For these spectra, the signal intensity is proportional to the X-ray photon count, and elements associated with each peak are shown. Peak maxima are located at 0.28 keV for carbon, 0.40 keV for nitrogen, and 1.76 keV for silicon, which is in good agreement with values tabulated elsewhere.[25] At a 2 min exposure time, only silicon and nitrogen are detected, as expected for silicon nitride. After 20 min of scanning, a carbon peak is clearly present while traces of oxygen remain low. A full quantitative analysis of these spectra is not straightforward; however it is possible to qualitatively determine any increase in carbon contamination by observing the variation in peak heights.[25] Since the absolute photon count depends on the exact acquisition time, the relative heights of the maxima associated with carbon, nitrogen, and silicon were compared. The variation in the ratios of the carbon-to-silicon peaks and the nitrogen-to-silicon peaks as a function of time are presented

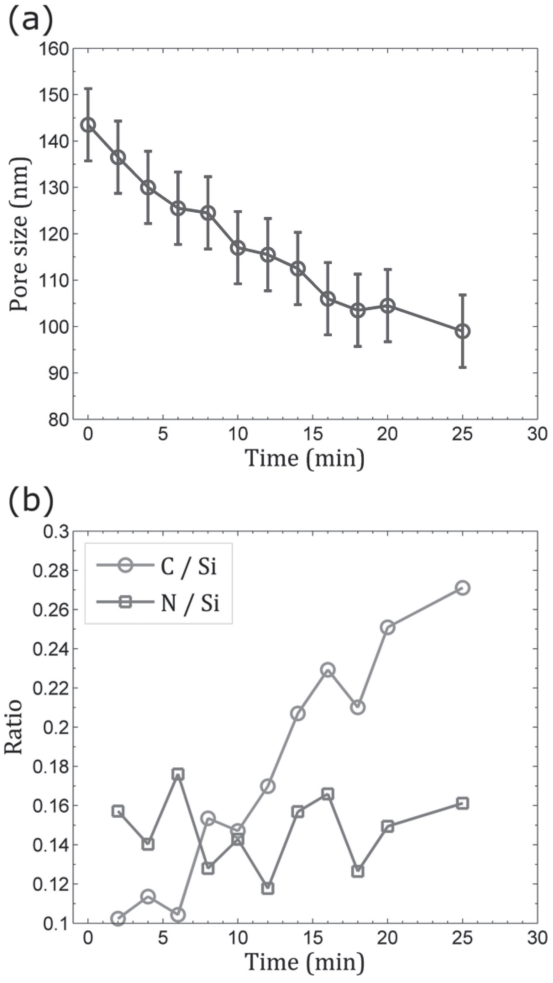

Figure 2. a) Evolution of pore size (diameter) during electron exposure of the Si_3N_4 pore. Error bars correspond to the estimated measurement uncertainty (±8 nm). b) Corresponding ratios of element-assigned peaks in EDX spectra. The levels of carbon and nitrogen are shown as the normalized peak heights of these elements relative to that of silicon.

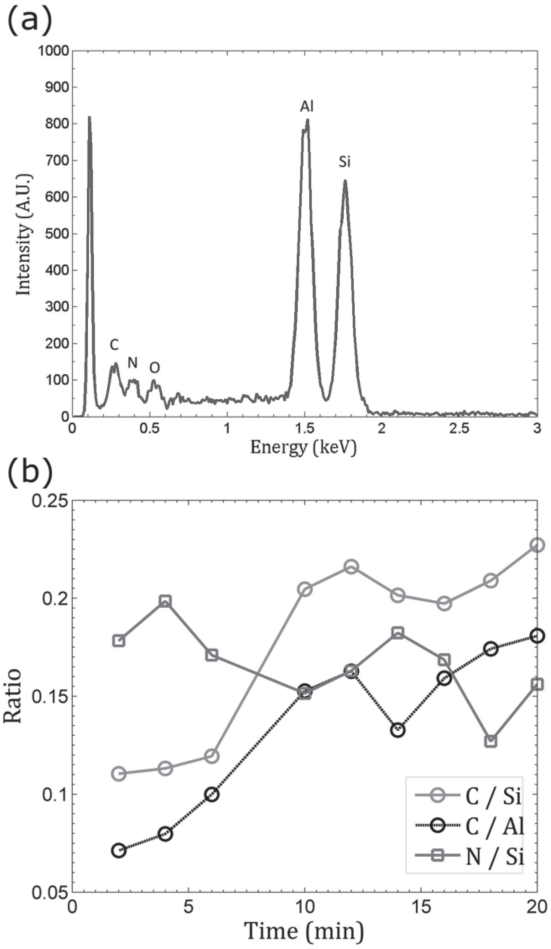

Figure 3. a) EDX spectrum and b) ratios of element-assigned EDX peaks for an aluminium coated membrane. The spectrum was acquired after 20 min electron exposure and at a 20° tilt angle.

in **Figure 2**b. There is an overall increase in the level of carbon as the pore diameter decreases, whereas the level of nitrogen (the control measurement) does not show any particular trend. The pore shrinkage rate can be estimated using linear fits of the pore diameters measured with SEM. It is apparent from Figure 2a, however, that the shrinkage rate is not constant throughout the process. During approximately the first 6 min of beam exposure the shrinkage rate is steady at 3.1 ± 0.3 nm min^{-1}. After this period, the shrinkage rate decreases gradually, so that the shrinkage rate, averaged over the full 25 min, is only 2.1 ± 0.4 nm min^{-1}. This behavior is consistent with that observed by Kox et al., who attributed the variation to diffusion and gradual depletion of the precursor gas.[21]

In order to verify that carbon deposition also occurs with coated membranes, a similar procedure was applied to membranes consisting of 60 nm Si_3N_4 and 100 nm-thick Al. For in-situ EDX measurements, it was necessary to tilt the device by 20° to avoid obstruction of the X-ray path by the back-etched window structure in which dual-layer membranes were mounted. **Figure 3**a shows EDX data acquired by scanning the Si_3N_4 side of the device, with an aluminium peak clearly detectable at 1.52 keV. Figure 3b highlights the increase in the relative carbon peak (at 0.28 keV) magnitude during the 20 min of electron exposure, confirming carbon deposition.

Next, shrinking on the aluminium side was confirmed by comparing a shrunk sample with an identically milled reference pore. Once again the sample undergoing shrinking was tilted at 20° to the e-beam for the purposes of EDX measurements. The pore was scanned on the Si_3N_4 side for 10 min, during which there was 14 nm shrinkage (an average shrinkage rate of 1.4 ± 0.5 nm min^{-1}) and an increase in the carbon peak (**Figure 4**). The device was then imaged on the aluminium side. Compared to the reference pore milled with the same FIB parameters but not resized with SEM, the shrunken pore was ≈28 nm smaller, implying that the shrinkage rate was higher on the unexposed side. This observation can be explained (but not quantified) by a difference in the availability of hydrocarbons or secondary electron yields on each side of the membrane.

A further set of experiments was undertaken using a nanopore array in order to test the effect of different initial pore sizes and SEM parameters on both shrinkage rate and carbon deposition. Here the membrane contains seven pores (labeled sequentially P1–P7), with four pores (P1–P4) exposed

NANO MICRO small

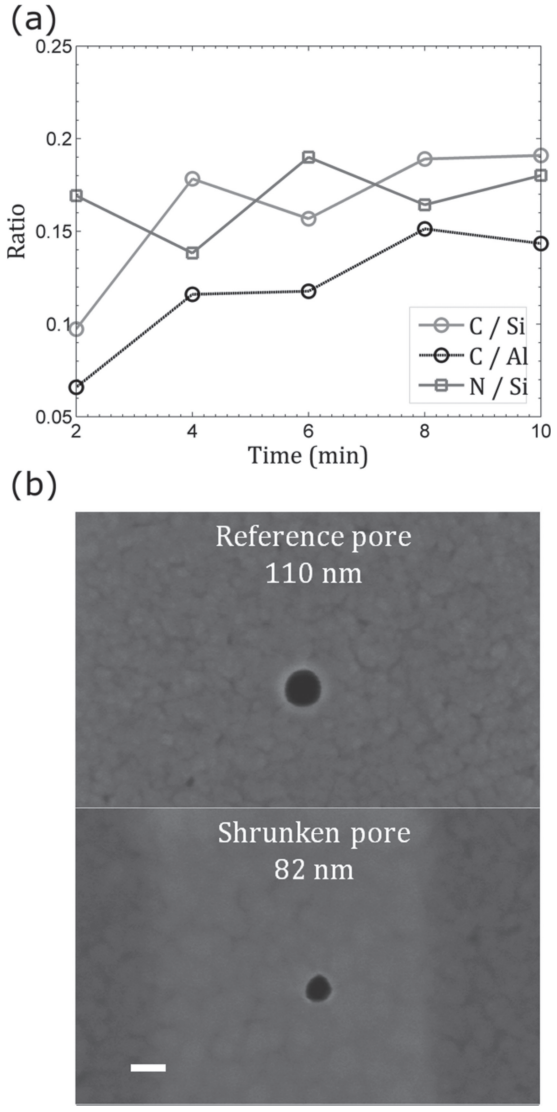

Figure 4. a) Ratios of element-assigned EDX peaks over 10 min of electron exposure (at tilted angle) and b) SEM images of the aluminium side of a reference pore (no shrinking) and a shrunken pore. The scale bar represents 100 nm.

to electron irradiation, while the other three (P5–P7) serve as references. In this case, the device was not tilted, allowing more uniform carbon distribution around the pores, and EDX spectra were only acquired after shrinking. Scanning area, beam voltage, and exposure times were varied and are summarized in **Table 1**. The average shrinkage rates over the entire process are also presented for each case.

It was observed that the Al/Si_3N_4 pores shrank significantly faster with a beam voltage of 20 kV than at 5 kV. At 5 kV, the secondary electron yield should be greater than at 20 kV for both Al and Si_3N_4,[24,26] so it is unlikely that this trend is associated with the EBID process, and instead may be linked to a change in one of the other system properties, such as a reduction in primary electron current. For these cases, the relative shrinkage rates of the aluminium and Si_3N_4 layers were found to be variable. At 5 kV, shrinking was more efficient on the metal side (P1 and P2), whereas at 20 kV, the shrinking was similar on both sides (P3) or slightly greater on the Si_3N_4 layer (P4). As with previous studies,[21] there was considerable variation in resizing behavior between individual pores at the same voltage. As mentioned above, pore shrinking is sensitive to the quantity of available hydrocarbon resist. It was noted that the pressure in the vacuum chamber (3.70×10^6 mbar) was slightly higher for the cases in Table 1 than in the earlier experiments (around 2.90×10^6 mbar), indicating that the quantity of contamination resist available when shrinking P4 is likely to have been greater.

Despite the presence of carbon deposition over the scanned region, images of the pores suggest that other mechanisms may contribute to pore shrinkage. **Figure 5** illustrates pores before and after shrinking, as well as the pore appearance on the Al side of the membrane. The images reveal some granularity on the Si_3N_4 side of P2 and P3 which was not present before pore shrinkage. These two pores were scanned over a smaller area than P1 and P4, although at the same magnification. On P3 it is noticeable that the lighter carbon film clearly follows the contour of the scanning rectangle but the grain pattern is only located around the pore. The granular appearance around some of the shrunken pores (e.g., in Figure 5) cannot be explained by the deposition of a carbon film, and there may therefore be an additional process competing with deposition, e.g., electron-stimulated desorption.[27] If the observed grain is the aluminium layer, then the hole in the Si_3N_4 layer must have expanded beyond its original size. This proposed mechanism is similar to the resizing of nanopores inside a TEM, where pores with large aspect ratios (pore diameter to membrane thickness) have been found to expand under the influence of the electron beam.[6,28] Nevertheless, EDX spectra consistently show that the shrunken pores have enhanced carbon levels compared to the unexposed pores (**Figure 6**).

Pore shrinking of FIB-milled nanopores using low energy electrons is advantageous because SEM systems are both common and inexpensive, while offering superior imaging resolution to FIB. In their report, Zhang et al. suggested that pore shrinking in Si_3N_4 membranes could be due to a combination

Table 1. Parameters used for the shrinking of P1, P2, P3, and P4, with calculated shrinkage rates.

Pore	Initial diameter [nm]	Voltage [kV]	Scan area [nm^2]	Time [min]	Final diameter, Si_3N_4 [nm]	Final diameter, Al [nm]	Average shrinkage rate, Si_3N_4 side [nm min^{-1}]
P1	125	5	894 × 671	3	113	89	4.0
P2	65	5	305 × 228	5	60	45	1.0
P3	107	20	305 × 228	5	34	71	14.6
P4	114	20	894 × 671	7	53	52	8.7

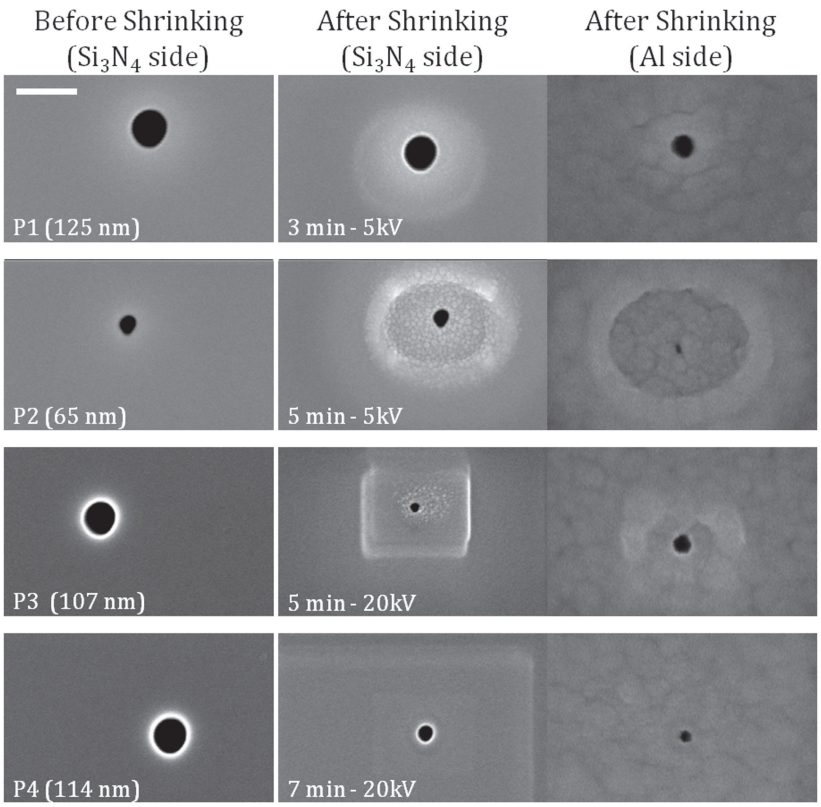

Figure 5. SEM images of pores P1, P2, P3, and P4 before and after shrinking. The third column shows the pore on the metalized side after shrinking. The scale bar represents 200 nm.

of Joule heating and electron beam-induced migration, however, they did not consider any type of deposition process.[23] In another experiment with SiO_2, Chang et al. tested for the presence of carbon by argon–oxygen plasma cleaning and electron energy loss spectroscopy (EELS), and concluded that the shrinkage process was not associated with carbon deposition.[22] However, in the present study, there is a noticeable increase in the level of carbon on the specimen for all cases, regardless of beam and scanning parameters. If the shrinkage process was entirely due to migration, then thinning of the nitride and flow through the pore should have been observed. Instead, in both Figure 4 and 5 it is possible to see the rectangular 'footprint' of the SEM scan on the aluminium, illustrating that deposition of carbon occurred simultaneously on both sides of the membrane. It can therefore be concluded that pore shrinking on both sides is in part due to carbon deposition, as suggested by previous reports.[20,21]

As a further comment, it was observed that the resized pores demonstrate remarkable resistance to cleaning. In their experiments on silicon pores, Kox et al. found that the carbon deposits were resistant to organic solvents and piranha solution, but not to 2 min dry cleaning with an O_2 plasma.[21] In contrast, after 4 min in a H_2/O_2 plasma cleaner specially designed for carbon removal (Solarus 950, Gatan Inc.), the pores in Figure 5 did not revert to their original sizes. Furthermore, attempts to dissolve the carbon deposits in hexane or acetone did not result in any change. The resistance of the shrunken pore to H_2/O_2 plasma cleaning specifically indicates that the deposited carbon compound may not be the same as that observed by Kox et al. Although the composition of the deposit is usually C_9H_2O, a more stable structure may result from electron exposure.[29] While it is highly promising that pore size was reduced for all Al-coated membranes, the predominant role of carbon deposition in the pore-shrinking process has consequences for the reliability of SEM-based fabrication techniques. The shrinkage rate depends on the availability of the precursors in the vacuum chamber, and is therefore likely to vary with time, as demonstrated in the current study and that of Kox et al.[21] EBID process outcomes are dependent on a number of parameters, so optimizing precursor and beam conditions for the two layers (e.g., via a gas-injection system) will improve the repeatability of pore shrinking in these membranes.

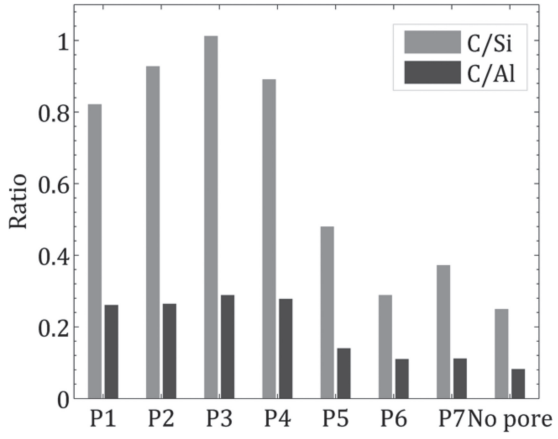

Figure 6. Relative magnitude of the carbon peak in EDX spectra (in relation to the silicon or aluminium peak magnitude) for different pores (P1–P4) shrunk using different beam parameters, compared with three reference pores (P5–P7) and a region with no pore. The shrunken pores (P1–P4) all exhibit increased carbon levels.

3. Conclusion

In summary, an SEM electron beam has been used to shrink nanopores in both uncoated Si_3N_4 membranes and Si_3N_4 membranes coated with a thin aluminium layer. In addition to pore shrinking, carbon deposition in the vicinity of the pore should act as a good insulating layer for protecting the Al from the solution or analyte molecules. The procedure was repeated successfully on a range of samples with different initial pore sizes and various SEM scanning conditions. Imaging revealed that the aluminium side of the pores shrank simultaneously with the Si_3N_4 side. In all cases pore reduction was achieved, although the average shrinkage rate varied

NANO MICRO small

between approximately 1.0 and 14.6 nm min^{-1}, the relative shrinkage rates of the two layers was dependent on the SEM conditions, and the instantaneous shrinkage rate decreased during pore exposure. EDX spectra acquired at various stages of the shrinkage process consistently revealed the presence of carbon in the pore region, providing evidence that SEM-induced pore shrinking occurs at least partly due to a deposition process. SEM imaging also illustrated the presence of carbon, as well as additional granular structures on the membrane surface in the vicinity of the pores, which may be due to a separate thinning process. Further work is required to improve the repeatability of the SEM-based technique where accurate, 'single-digit' pores are required, as well as confirming the geometry of the internal pore shape. Nevertheless this appears to be a direct and useful approach for shrinking nanopores in multilayered membranes.

4. Experimental Section

The nanopore devices consisted of milled, free-standing Al/Si_3N_4 membranes centered on a silicon substrate. The fabrication process has been described in detail elsewhere.[4] Firstly, a 60 nm-thick Si_3N_4 layer was deposited onto both sides of a silicon wafer by low-pressure chemical vapor deposition (LPCVD). Next, a photoresist was spun onto the back side of the wafer in order to pattern a 50 μm × 50 μm window using photolithography. This pattern was then transferred to the bottom Si_3N_4 layer by reactive ion etching (RIE) and then the silicon layer via KOH wet-etching. A metal layer was deposited onto some membranes by thermal evaporation. For the current work, a 100 nm-thick aluminium layer was used.

After metallization, cylindrical nanopores were milled with a focused ion beam with an acceleration voltage of 30 kV. Beam currents and milling times were adjusted to control pore size, with low currents (<10 pA) used to achieve high resolution. The FIB system (Carl Zeiss XB1540) was equipped with both an electron and a gallium ion gun tilted at an angle of 54° from each other. This facilitated FIB milling, SEM pore shrinking, and SEM imaging processes within a single system. Pore dimensions were measured by SEM imaging after milling and during resizing. For this process, acceleration voltages of 5 and 20 kV were used, which provided suitable image contrast without excessive charging effects at these magnifications. Pore diameters were measured to an accuracy of ±3 pixels, which corresponded to ±8 nm at a magnification of 100 000×.

EDX was used to investigate the presence of carbon during pore shrinking.[21] As the same electron beam was used for scanning and EDX, it was possible to record the level of carbon while the SEM was shrinking the nanopore. For these experiments, a detector (EDAX Sapphire) was inserted inside the SEM chamber and commercial software (Genesis) was used to acquire the spectra.

Acknowledgements

This work has been supported in part by the EPSRC, Leverhulme Trust, and HFSP. The authors thank A. P. Ivanov for useful discussions.

[1] C. Dekker, *Nat. Nanotechnol.* **2007**, *2*, 209.
[2] S. Howorka, Z. Siwy, *Chem. Soc. Rev.* **2009**, *38*, 2360.
[3] A. P. Ivanov, E. Instuli, C. M. McGilvery, G. Baldwin, D. W. McComb, T. Albrecht, J. B. Edel, *Nano Lett.* **2011**, *11*, 279.
[4] G. A. T. Chansin, R. Mulero, J. Hong, M. J. Kim, A. J. deMello, J. B. Edel, *Nano Lett.* **2007**, *7*, 2901.
[5] J. Hong, Y. Lee, G. A. T. Chansin, J. B. Edel, A. J. DeMello, *Nanotechnology* **2008**, *19*, 165205.
[6] A. J. Storm, J. H. Chen, X. S. Ling, H. W. Zandbergen, C. Dekker, *Nat. Mater.* **2003**, *2*, 537.
[7] J. B. Heng, C. Ho, T. Kim, R. Timp, A. Aksimentiev, Y. V. Grinkova, S. Sligar, K. Schulten, G. Timp, *Biophys. J.* **2004**, *87*, 2905.
[8] M. J. Kim, B. McNally, K. Murata, A. Meller, *Nanotechnology* **2007**, *18*, 205302.
[9] M. J. Kim, M. Wanunu, D. C. Bell, A. Meller, *Adv. Mater.* **2006**, *18*, 3149.
[10] D. Krapf, M.-Y. Wu, R. M. M. Smeets, H. W. Zandbergen, C. Dekker, S. G. Lemay, *Nano Lett.* **2005**, *6*, 105.
[11] M. Ayub, A. P. Ivanov, J. Hong, P. Kuhn, E. Instuli, J. B. Edel, T. Albrecht, *J. Phys.: Condens. Matter* **2010**, *22*, 454128.
[12] M. Ayub, A. P. Ivanov, E. Instuli, M. Cecchini, G. Chansin, C. McGilvery, J. Hong, G. Baldwin, D. McComb, J. B. Edel, T. Albrecht, *Electrochim. Acta* **2010**, *55*, 8237.
[13] G. V. Soni, A. Meller, *Clin. Chem.* **2007**, *53*, 1996.
[14] J. Li, D. Stein, C. McMullan, D. Branton, M. J. Aziz, J. A. Golovchenko, *Nature* **2001**, *412*, 166.
[15] J. R. Lakowicz, *Principles of Fluorescence Spectroscopy*, Springer, New York **2006**.
[16] S. J. Randolph, J. D. Fowlkes, P. D. Rack, *Crit. Rev. Solid State Mater. Sci.* **2006**, *31*, 55.
[17] C. Danelon, C. Santschi, J. Brugger, H. Vogel, *Langmuir* **2006**, *22*, 10711.
[18] W. W. Molzen, A. N. Broers, J. J. Cuomo, J. M. E. Harper, R. B. Laibowitz, *J. Vac. Sci. Technol.* **1979**, *16*, 269.
[19] A. Radenovic, E. Trepagnier, R. Csencsits, K. H. Downing, J. Liphardt, *Appl. Phys. Lett.* **2008**, *93*, 183101.
[20] T. Schenkel, V. Radmilovic, E. A. Stach, S.-J. Park, A. Persaud, *J. Vac. Sci. Technol., B: Microelectron. Nanometer Struct.* **2003**, *21*, 2720.
[21] R. Kox, C. Chen, G. Maes, L. Lagae, G. Borghs, *Nanotechnology* **2009**, *20*, 115302.
[22] H. Chang, S. M. Iqbal, E. A. Stach, A. H. King, N. J. Zaluzec, R. Bashir, *Appl. Phys. Lett.* **2006**, *88*, 103109.
[23] W. M. Zhang, Y. G. Wang, J. Li, J. M. Xue, H. Ji, Q. Ouyang, J. Xu, Y. Zhang, *Appl. Phys. Lett.* **2007**, *90*, 163102.
[24] W. F. van Dorp, C. W. Hagen, *J. Appl. Phys.* **2008**, *104*, 081301.
[25] J. Goldstein, D. Newbury, D. Joy, C. Lyman, P. Echlin, E. Lifshin, L. Sawyer, J. Michael, *Scanning Electron Microscopy and X-ray Microanalysis* Kluwer Academic/Plenum Publishers, New York **2003**.
[26] L. Reimer, *Scanning Electron Microscopy*, Springer-Verlag, Berlin **1998**.
[27] R. D. Ramsier, J. T. Yates, *Surf. Sci. Rep.* **1991**, *12*, 246.
[28] J. W. Shin, J. Y. Lee, D. U. Lee, D. H. Oh, D. H. Kim, T. W. Kim, W. J. Cho, S. Jin, *Nanotechnology* **2009**, *20*, 075703.
[29] I. Utke, P. Hoffmann, J. Melngailis, *J. Vac. Sci. Technol., B: Microelectron. Nanometer Struct.* **2008**, *26*, 1197.

Received: May 25, 2011
Revised: June 24, 2011
Published online: August 24, 2011

